Ionics (2021) 27:1795–1802
https://doi.org/10.1007/s11581-021-03911-7

ORIGINAL PAPER

Nanocomposites prepared from gold nanowires and multiwalled carbon nanotubes for non-enzymatic sensitive bioelectrochemical detection of pentraxin-3 in human serum

Qiongyuan Zhang[1] · Jiayi Wu[1] · Wuceng Niu[1] · Jianjiang Xue[1]

Received: 6 February 2020 / Revised: 16 December 2020 / Accepted: 12 January 2021 / Published online: 27 January 2021

Abstract

Pentraxin-3 (PTX-3) is one of the newly discovered tumor biomarker, especially in the diagnosis of lung cancer. The functionalized multi-walled carbon nanotubes (MWCNTs) and gold nanowires (AuNWs) nanocomposites decorated the PTX-3 biosensor were reported in this work, realizing ultrasensitive detection of PTX-3 in human serum through simple and effective non-enzymatic reaction. The PTX-3 biosensor has excellent electrochemical activity and biocompatibility through carbon and metal nanomaterials. Compared with pure MWCNTs, the MWCNTs combined with AuNWs which shows a wide range of detection (0.001–1000 ng ml^{-1}), higher sensitivity (17.10 μA/(ng ml^{-1})/cm^2) and lower detection limits (0.16 pg ml^{-1}, S/N = 3). Meanwhile, gold nanomaterials are one of the most stable noble metal nanomaterials and MWCNTs possess large electroactive surface area, which can greatly improves the stability (96.3%, after 3 weeks) and repeatability (RSD = 0.51%). This work remarkably extends the utilization of MWCNTs and AuNWs in the construction of biosensors in the fields of biosensing and medical diagnosis.

Keywords Glassy carbon electrode · Gold nanowires · Multi-walled carbon nanotubes · Pentraxin-3 · Biosensor · Nanocomposite

Introduction

Carbon is an important element in extensive scientific research in various sciences, and carbon nanotubes (CNTs) have received great attention. CNTs have unique electrical, mechanical, and surface properties [1–3], and can be divided into single-walled carbon nanotubes and multiwalled carbon nanotubes (MWCNTs), in which MWCNTs can be seen as composed of multi-layer graphene crimp [4, 5]. CNTs are tubular structures, have sufficiently high strength, excellent thermal, and chemical properties, smaller density than graphene. Thus, CNTs have great potential in biomedical applications [6–8]. CNTs have excellent electrochemical activity, biocompatibility, and large specific surface area, which can be used as a biomolecule immobilized carrier and an ideal electron transfer medium to construct an electrochemical sensor [9, 10]. CNTs can also be used to improve the performance of polymer composites, especially in combination with noble metal nanomaterials, which can significantly improve the analytical performance of the sensor [11, 12]. Gold-based structures such as gold nanoparticles and gold nanowires (AuNWs) have been extensively used in the construction of sensing devices in the field of chemistry and biochemistry, where gold nanowires have excellent optical, electrical, and mechanical properties [13–15]. As a one-dimensional metal nanostructure, AuNWs can synthesize different aspect ratios according to different strategies, with vertical dimensions up to several tens of microns [16–18]. It has the advantages of high aspect ratio, large specific surface area, and anisotropy, and also has good biocompatibility. Metal-doped CNTs are potential materials for electrochemical sensors and a variety of biomedical applications, which can obviously enhance the sensing performance and the conductivity of the electrochemical sensors. Moreover, it also shows an excellent stability and repeatability [19–21].

Pentraxin-3 (PTX-3) acts as a soluble pattern recognition receptor in the innate immune response, which is also important for acute inflammation period response protein [22, 23]. In the past decade, PTX-3 has emerged as a candidate new biomarker of inflammation, including clinical use of cancer-related inflammation [24], especially lung cancer [25], as it better reflects local and systemic inflammatory processes compared with other

✉ Jianjiang Xue
jianjiangxue@163.com

[1] Department of Clinical Laboratory, The University-Town Affiliated Hospital of Chongqing Medical University, No. 55 The University-Town Middle Road, ShaPingBa District, Chongqing 401331, China

inflammation markers. The level of PTX-3 is low (< 2 ng ml^{-1}) in normal human, and PTX-3 rapidly (6 ~ 8 h after induction peak) significantly increased (up to 200–800 ng ml^{-1}) in the inflammatory and infection [26]. Meanwhile, PTX-3 is overexpressed in some malignancies, and the serum level is associated with the severity of the disease [27, 28].

Many analytical techniques have been developed for the detection of serum PTX-3 levels, including chemiluminescence [29], enzyme-linked immunosorbent assays (ELISA) [30], radioimmunoassay [31], and mass spectrometry [32]. These conventional detection techniques are widely used, but each has its advantages and disadvantages, the most obvious of which is the need for expensive instruments and complex operating procedures. In addition, ELISA is a universal method based on antigen-antibody specific recognition, which is widely used in clinical testing. However, this method is affected by a number of factors, which would be resulted it in a lower sensitivity. Undoubtedly, simple, fast, and sensitive detection methods are more beneficial for PTX-3 detection. Based on this, we aimed to develop a highly sensitive, easy to operate biosensor to successfully avoid the drawbacks of current clinical testing methods. With the continuous development of biosensors, electrochemical methods have strong appeal and the ability to detect different types of biomarkers [33, 34]. For example, electrochemical sensor with MWCNTs-chitosan has been used to determine the indole in plasma [35], an electrochemical immunosensor with Fe_3O_4@Au for detection of alpha fetoprotein [36] and the poly (2-aminothiophenol)-Au nanoparticles modified gold electrode to fabricate an electrochemical immunosensor for carcinoembryonic antigen detection [37]. In addition, label-free non-enzyme detection can also be applied to the development of cell capture technology, which is also a new method in the application of biological detection and analysis [38, 39].

In this paper, we demonstrated a novel non-enzymatic electrochemical biosensor platform that combined the unique properties of functionalized MWCNTs and AuNWs for the ultrasensitive detection of serum PTX-3. MWCNTs-AuNWs nanocomposites possess a larger surface area, significant electrocatalytic activity, and good stability, which would immobilize more biomolecules, improving the electrochemical signal of the biosensor effectively. A remarkably simple and one-step functionalization of the nanocomposites was developed for immobilization of anti-PTX-3 antibody and it can directly detect the PTX-3 antigen content by the specificity recognition between the antigen and the antibody. Differential pulse voltammetry (DPV) is one of the effective techniques for analyzing the kinetic transduction mechanism of PTX-3 antigen-antibody interactions. This is an electrochemical biosensor that used MWCNTs-AuNWs nanocomposites to directly detect PTX-3 antigens, which shows high sensitivity for the quantitative determination of PTX-3 in human serum and has considerable potential in clinical and diagnostic applications.

Experimental

Chemical and reagents

MWCNTs (outside diameter: 7–15 nm) were purchased from Shenzhen Nanotech Port Ltd. Co. (Shenzhen, China). The bare AuNWs (≥ 50 μg ml^{-1}) at 30.0 nm diameter and 4500.0 nm length (aspect ratio of approximately 150) that was in distilled water with excess CTAB capping agent, 1-ethyl-3-(3-dimethyllaminopropyl) carbodiimidehydrochloride (EDC), *N*-hydroxysuccinimide (NHS), bovine serum albumin (BSA),and *N*,*N*-dimethylformamide (DMF) were obtained from Sigma-Aldrich (USA). PTX-3 and anti-PTX-3 were purchased from Sino Biological Port, Ltd., Co. (Beijing, China). 0.01 M phosphate-buffered saline (PBS) was prepared in Millipore-Q water (≥ 18.2 MΩ) as washing buffer, contained 2.7 mMKCl, 14 mM KH_2PO_4, 87 mM Na_2HPO_4,and 136.7 mM NaCl (pH 7.4). The remaining materials were received without further purification and purchased in analytical grade from Chuandong Chemical (Group), Ltd., Co. (Chongqing, China).

Synthesis of functionalized MWCNTs and MWCNTs-AuNWs nanocomposites

The MWCNTs (10 mg) was added to 100 ml of concentrated HCL and heated under reflux with magnetic stirring for 8 h to remove the metal catalyst. The purified MWCNTs were placed in 100 ml of concentrated mixture acids (HNO_3:H_2SO_4 = 1:3, v/v) and ultrasonicated at room temperature for 10 h. After completion of the ultrasonication, it was washed with distilled water until neutral to obtain the short carboxylated MWCNTs (COOH-MWCNTs) and stored after it was dried.

The COOH-MWCNTs (0.5 mg ml^{-1}) was dispersed in DMF for 30 min by ultrasonication to form a homogeneous and stable slurry solution. Then, the AuNWs solution (AuNWs:COOH-MWCNTs = 1:1, v/v) was added and stirred at room temperature for 12 h to obtain MWCNTs-AuNWs (MAuNWs), which were stored at 4 °C prior to use.

Fabrication of the electrochemical biosensor

The GCE (φ = 3 mm) is used as working electrode. It was polished with 0.03 μm and 0.05 μm alumina slurry on a microcloth polishing pad until mirror-like. Then, it was washed with ethanol and deionized water and dried with nitrogen. Finally, the functionalized MAuNWs were carefully dropped on to the surface of the cleaned GCE, and the electrodes were dried at a room temperature to obtain MAuNWs/GCE. For comparison, the COOH-MWCNTs electrode was prepared by the same procedure.

Prior to anti-PTX-3 antibody immobilization, the prepared electrodes were treated with EDC-NHS cross-linked solution for 2 h to activate the -COOH groups of the MWCNTs to be

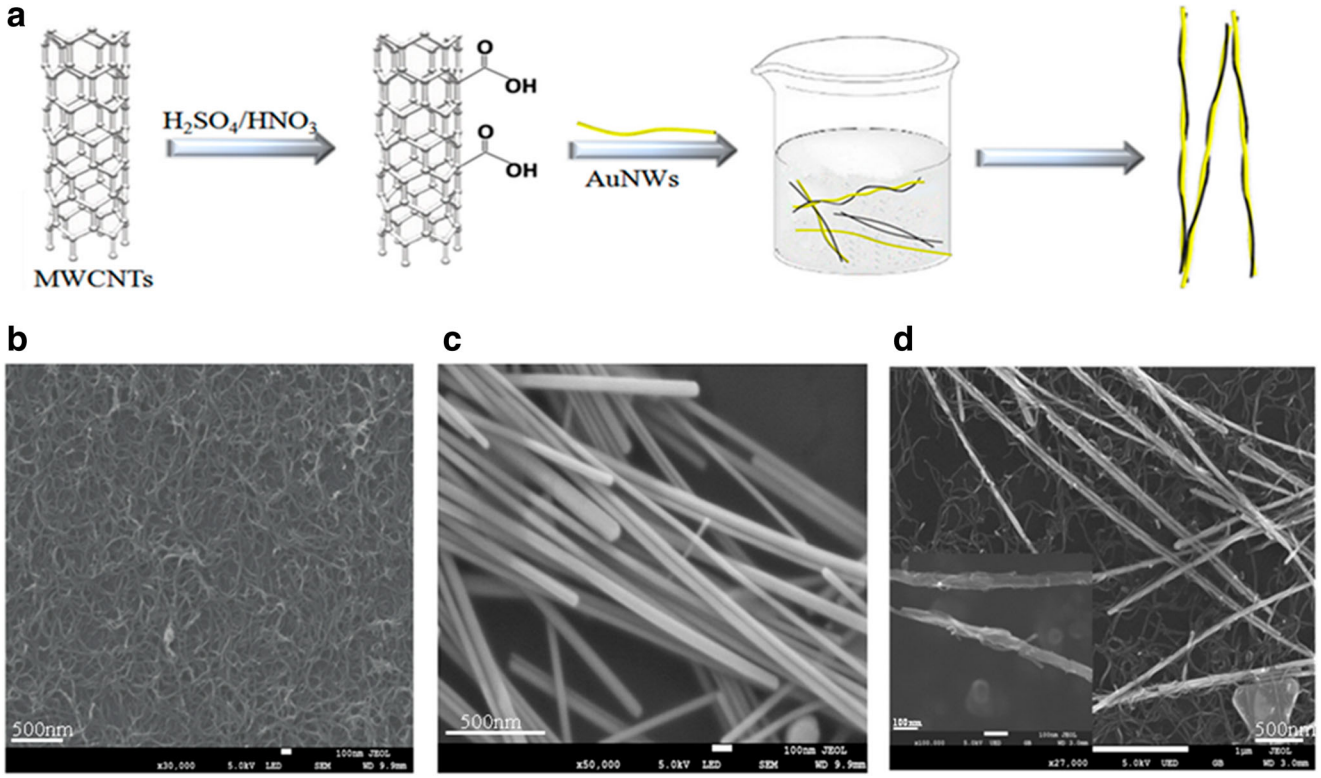

Fig. 1 **a** The synthesis of the MWCNTs-AuNWs nanocomposites, FE-SEM image of **b** MWCNTs, **c** AuNWs, **d** MWCNTs-AuNWs nanocomposites

converted to -NH_2 groups. EDC/NHS (4 mM: 1 mM) cross-linked solution was prepared in PBS buffer. After completion of the activation, 10 μL of anti-PTX-3 antibody (200 ng ml^{-1}) was dropped onto the electrode surface and incubated overnight at 4 °C. The antibody can be covalently attached to the surfaces by -COOH with -NH_2 of MWCNTs, and AuNWs can also promote Au-S interaction with the thiol groups of the antibody Cys residue, thereby increasing the affinity of the anti-PTX-3 antibody to the MAuNWs. Subsequently, 10 μL of the BSA (1%) solution was dropped onto the electrode surface and incubated at 37 °C for 1 h to eliminate the unbound non-specific binding sites. The electrodes were washed thrice with PBS buffer before each step to remove unbound reagents. The prepared BSA/anti-PTX-3/MAuNWs/GCE electrode was stored at 4 °C before further use. Meanwhile, the BSA/anti-PTX-3/MWCNTs/GCE electrode was prepared using the same preparation strategy.

Electrochemical measurements

The electrochemical measurement was performed using a three-electrode system consisting of Ag/AgCl saturated with KCl as the reference electrode, the platinum wire as the auxiliary electrode, and the modified GCE as the working electrode. The electrochemical workstation AUTOLAB PGSTAT302 (Metrohm Technology Co., Ltd., Switzerland) was used as a redox probe in 0.01 M phosphate-buffered saline (PBS, pH 7.4) containing 5 mM $[Fe(CN)_6]^{3-/4-}$. Cyclic voltammetry (CV, a potential range of − 0.1 V to 0.6 V at 50 mV s^{-1}) and electrochemical impedance spectroscopy (EIS, applied frequency from 100000 to 0.1 Hz with 0.01 V amplitude) are used to characterize the progressive fabrication of immune electrodes. DPV (potential scan from − 0.25 V to 0.55 V with 0.005 V amplitude) was used for the assessment of different concentrations of biosensor. The electrochemical response of the PTX-3 antigen standard solution at a concentration of 0–1000 ng ml^{-1} was performed and the change in current was recorded as a function of the antigen concentration to develop a high sensitivity, high selectivity, low detection limit, and stable immunosensor. These external experimental parameters should be optimized, including (a) the antigen incubation time, (b) the temperature of experiment, and (c) pH value of supporting electrolyte. The results are presented in the "Supporting information" section (Fig. S-1). The following were optimized experimental conditions for satisfied results: (a) the antigen incubation time of 45 min, (b)the temperature of 37 °C, and (c) pH value of 7.5.

Results and discussion

Characterization of the structure and morphology

The synthesis process of MAuNWs is shown in Fig. 1a. Meanwhile, as seen from the images of the field emission scanning electron microscopy (FE-SEM, JSM-

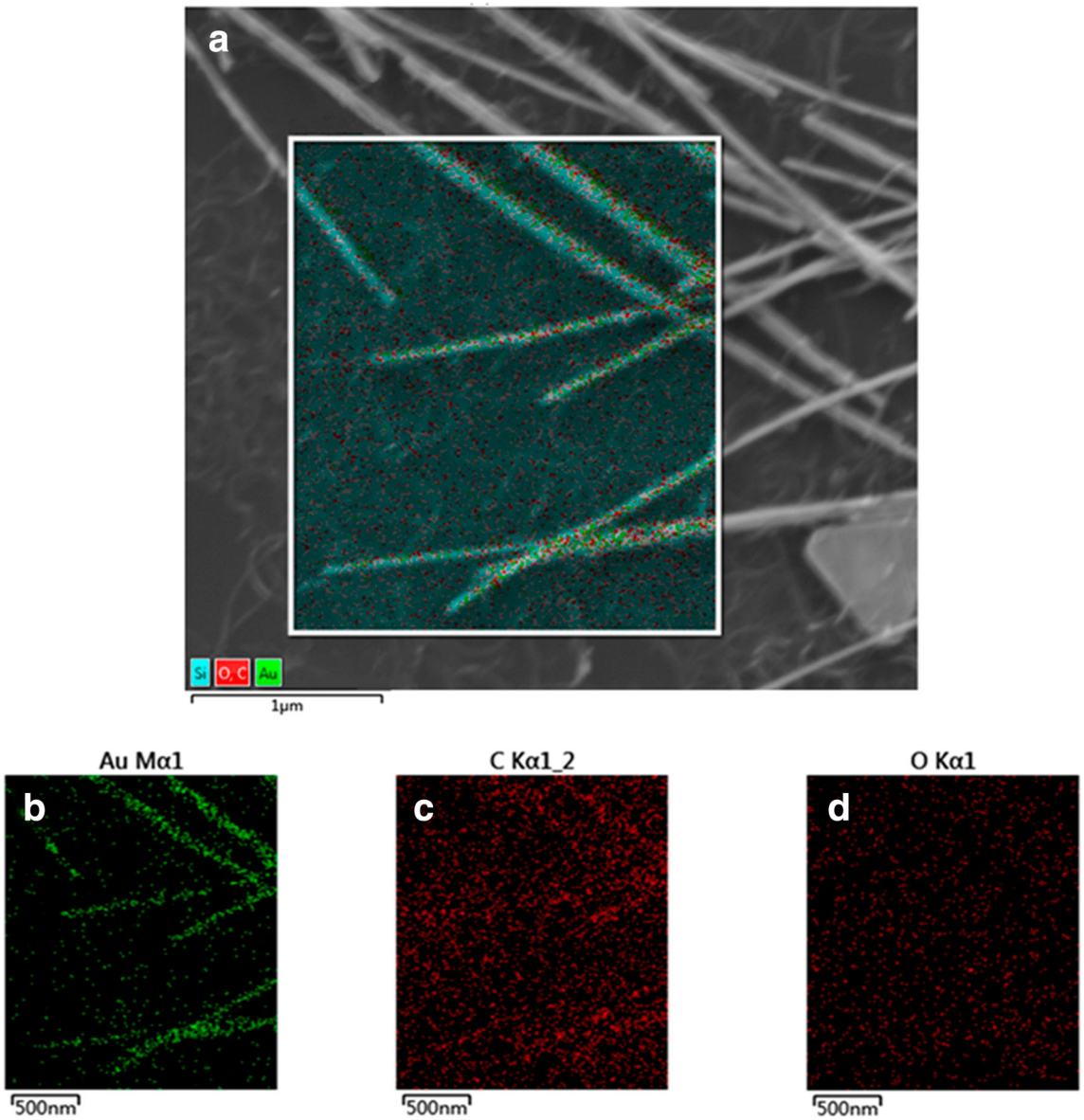

Fig. 2 **a** The EDS focus image of the MWCNTs-AuNWs nanocomposites. The EDS analysis of **b** Au, **c** carbon, **d** oxygen

7800F, JEOL, Japan), MWCNTs are uniformly and stably dispersed in DMF solution (Fig. 1b),the diameter and length of the bare AuNWs are consistent with the introduction of the chemical reagents (Fig. 1c), and MWCNTs and AuNWs are tightly complexed by physical adsorption (Fig. 1d). Figure 2a shows the focus image of MAuNWs along (energy dispersive X-ray spectroscopy, EDS, JSM-7800F, JEOL, Japan), which were presented Au (Fig. 2b), carbon (Fig. 2c), and oxygen (Fig. 2d).

Electrochemical behavior of the fabricated biosensor

The bioelectrochemical sensor self-assembly process is shown in Fig. 3a and the CV and EIS studies were conducted to elucidate the electrochemical behavior of various modified electrodes. Figure 3b shows the change in the current and potential of the electrodes under cyclic modification at a point in the range of − 0.1Vto 0.6 V, which is performed in a 5 mM $[Fe(CN)_6]^{3-/4-}$ solution. Compared with MWCNTs/GCE (curve b) electrode, the peak current of MAuNWs/GCE (curve c) electrode is obviously increased, and the current of the two electrodes is higher than that of the bare electrode (curve a). Compared with pure MWCNTs, MAuNWs provides an alternative conductive path because of the inclusion of AuNWs, thereby improving the electrical transfer kinetics. Subsequently, the successful addition of anti-PTX-3 antibody and BSA resulted in a significant reduction in current because of the reduced insulation performance of the protein and the further deterioration of the electrochemical current. EIS

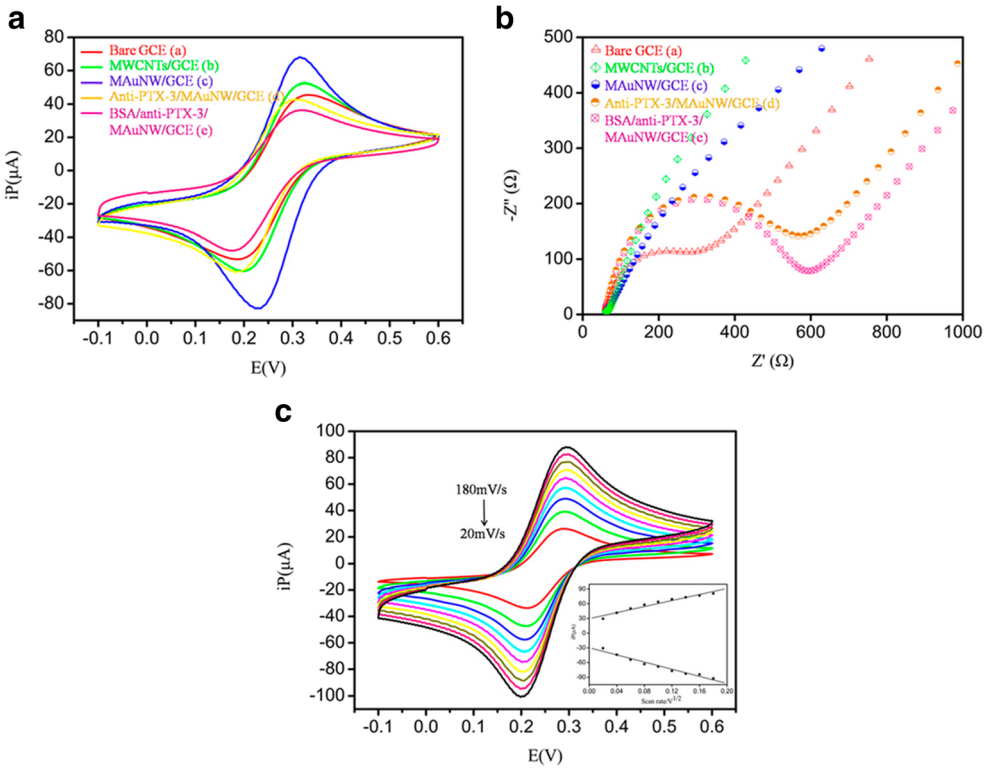

Fig. 3 **a** The fabrication of PTX-3 biosensor, **b** CV and **c** EIS responses of the different electrodes in 5 mM $[Fe(CN)_6]^{3-/4-}$ solution: bare GCE (curve a), MWCNTs/GCE (curve b), MAuNMs/GCE (curve c), anti-PTX-3/ MAuNMs/GCE (curve d), BSA/anti-PTX-3/ MAuNMs/GCE (curve e). **d** Anti-PTX-3/ MAuNMs/GCE at different scane rate (20–180 mV/s)

measured the charge transfer resistance of each assembled immunoelectrode; the greater the resistance, the greater the diameter of the semicircle was observed. The results of EIS (Fig. 3c) are consistent with CV, which confirms that the working principle of PTX-3 biosensor is consistent with the principle scheme.

Figure 3d shows the electrochemical behavior of the anti-PTX-3/MAuNWs immunoelectrode at a scanning rate of 20–180 mV/s. Redox currents move toward higher and lower potentials as the scan rate increases, and the curves of upper and lower are symmetrical, which indicating that this redox reaction is reversible. The linear changes in the peak current of the anode and cathode and the square root of the scanning rate indicate the diffusion process of electrons and follow the equation below.

$$I_a = 3.081 \times 10^{-4}\ \mathrm{A}\ (\mathrm{s\ mv^{-1}})\left[\text{scan rate}\ (\mathrm{mV\ s^{-1}})^{1/2}\right] + 2.968 \times 10^{-5}, R^2 = 0.97,$$

$$I_b = 3.652 \times 10^{-4}\ \mathrm{A}\ (\mathrm{s\ mv^{-1}})\left[\text{scan rate}\ (\mathrm{mV\ s^{-1}})^{1/2}\right] - 2.970 \times 10^{-5}, R^2 = 0.98.$$

Analytical performance of the biosensor for PTX-3

The electrochemical response characteristics of the prepared BSA/anti-PTX-3/MAuNWs immunoelectrode to the PTX-3 antigen concentration were obtained using DPV technique in a 5 mM $[Fe(CN)_6]^{3-/4-}$ solution (Fig. 4a). Figure 4b shows the DPV response of the

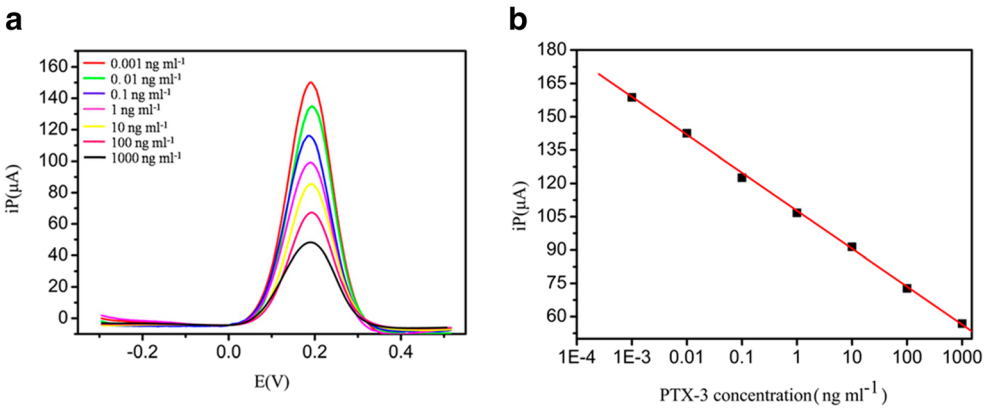

Fig. 4 **a** The sample preparation and detection process of the PTX-3 biosensor, **b** DPV analysis of the BSA/anti-PTX-3/MAuNMs/GCE biosensor for linear range concentration of PTX-3 antigen from 0.001–1000 ng ml^{-1}, **c** linear relationship between DPV peak current change vs. the logarithm of PTX-3 concentration

Table 1 Reproducibility of the BSA/anti-PTX-3/MAuNWs/GCE electrodes

Concentration (ng ml^{-1})	iP (A)			Mean	RSD (%)
	n_1	n_2	n_3		
0	1.7316E^{-04}	1.7341E^{-04}	1.7350E^{-04}	1.7336E^{-04}	0.10
0.1	1.2279E^{-04}	1.2243E^{-04}	1.2389E^{-04}	1.2304E^{-04}	0.62
1	1.0580E^{-04}	1.0504E^{-04}	1.0671E^{-04}	1.0585E^{-04}	0.79
10	9.1133E^{-05}	9.1380E^{-05}	9.1661E^{-05}	9.1391E^{-05}	0.29

immunized electrode with a target PTX-3 antigen concentration in the range of 0.001 ~ 1000 ng ml^{-1}. The peak current decreases with the increase in the target PTX-3 antigen concentration. This result may be due to the formation of immune complexes between the PTX-3 antigen and the anti-PTX-3 antibody, which increases the steric hindrance. Thus, redox and the diffusion of the probe toward the electrode surface are inhibited. At this concentration range, a good linear relationship exists between the current value and the logarithm of the concentration of PTX-3 antigen (Fig. 4c). The linear equation is ip (μA) = 107.719–17.1009log$C_{PTX\text{-}3}$; the correlation coefficient is 0.9997. The detection limit was obtained based on three times the standard deviation of the blank sample/slop and was calculated to be 0.16 pg ml^{-1}. In addition, it was observed that the response current of DPV tends to saturate at higher concentrations of PTX-3 antigen (after 1000 ng ml^{-1}) (Fig. S2). A controlled trial was conducted to examine the electrochemical response of the immunoreactive electrode that did not use anti-PTX-3 antibody to the PTX-3 antigen (Fig. S3). However, the corresponding current value of DPV did not change significantly (RSD = 0.0025) at different concentrations of PTX-3 antigen. The prepared BSA/anti-PTX-3/MWCNTs electrode was obtained using the same detection method to obtain the electrochemical response to the PTX-3 antigen concentration (0.1 ~ 1000 ng ml^{-1}), which showed narrow detection range and lower sensitivity (Fig. S4). Compared with other methods, this biosensor had a wider dynamic linear range and lower detection limit (Table S1).

Selectivity, reproducibility, and stability of the biosensor

To verify the selectivity of the biosensor to PTX-3 antigen, the potential effect of the interference on the sensor is a key factor in the preparation of the biosensor. Thus, the detection of interference is important. Using a mixture of interferons, such as BSA, hemoglobin (Hb), insulin-like growth factors-1 (IGF-1), C reactive protein (CRP), and the abovementioned interferants (Fig. S5a), the peak current change caused by the interferents (100 ng ml^{-1}) was less than 8% compared with the results obtained without using PTX-3 antigen (blank electrode). Meanwhile, the BSA/anti-PTX-3/MAuNWs immunoelectrode had a good response to the targeted PTX-3 antigen (10 ng ml^{-1}), and the peak current was significantly reduced. The results show that the prepared biosensor has good selectivity.

The reproducibility of the biosensor was evaluated under similar preparation conditions with the use of three immunoelectrodes prepared in the same batch. By detecting different concentrations of PTX-3 antigen, it can be seen that the relative standard deviation (RSD) is 0.10% ~ 0.79% (Table 1), indicating good reproducibility of the proposed biosensor (Fig. S5b).

To investigate the stability of BSA/anti-PTX-3/MAuNWs immunoelectrode, a test was performed every 1 week by detecting PTX-3 antigen (0.1 ng ml^{-1}) at an interval of 7 days to

Table 2 Recovery results of PTX-3 antigen in human samples using proposed biosensor

Sample	PTX-3 antigen concentration (ng ml^{-1})		Recovery (%)	RSD (%)
	Added	Found		
1	0	5.96 × 10^{-2}	0	1.61
2	0.01	9.91 × 10^{-2}	99.1	8.52
3	0.1	0.1	104.57	5.13
4	1	1.02	101.62	2.56
5	100	97.61	97.61	4.43
6	200	207.08	103.54	7

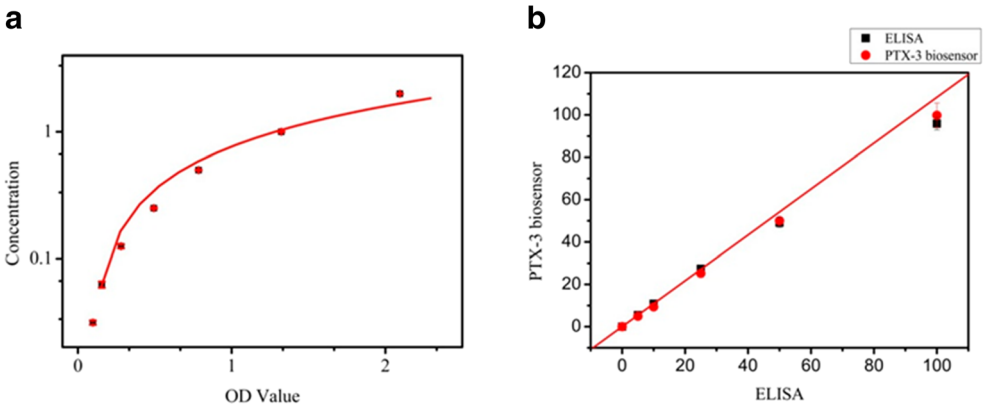

Fig. 5 **a** Regression of standard curve for ELISA, **b** comparing the detection of PTX-3 in serum samples by ELISA and PTX-3 biosensor

3 weeks (Table S2). The unused immune electrode was stored at 4 °C. The biosensor retained 96.3% of the initial current value after 3 weeks of storage (Fig. S6). The stability of the prepared biosensor is acceptable.

Real sample analysis

To assess the reliability and clinical feasibility of the proposed biosensor, the standard solution of the PTX-3 antigen was added to the collected serum sample, diluted to different concentrations of PTX-3 human serum samples, and prepared using a biosensor alone test. Each serum sample was tested at least three times and the recovery was calculated (Table 2). The results showed that the biosensor had a recovery rate of 97.61% ~ 104.57%, and RSD of 2.56% ~ 8.52%, thereby indicating that it had a good accuracy. In addition, five serum samples of different concentrations of PTX-3 antigen were prepared in parallel and divided into two groups. The results of the ELISA method were taken as reference values and the PTX-3 biosensor measured the results for comparison (Fig. 5a), analysis of electrochemical methods, and ELISA correlation (Table S3). The linear equation is $Y = 0.01744 + 1.08358 \times X$, and the linear regression coefficient is 0.999 (Fig. 5b), indicating that the two methods have good correlation. Therefore, the proposed PTX-3 biosensor is suitable for the detection of serum samples and provides a new method for the clinical study and detection of PTX-3.

Conclusion

In summary, MAuNWs nanocomposites biosensor is ultrasensitive, simple, and efficient for the label-free detection of PTX-3 antigens. AuNWs and MWCNTs can provide dual conductive paths to improve the conductivity of the biosensor, while functional groups on the surface of the electrodes can further improve the biosensor's biocompatibility. One-step synthesis of MAuNWs hybrid nanocomposites can directly fix the material with highly efficient electrocatalytic active on the electrode surface, which avoids the addition of other electrocatalytic substances in the detection solution to simplify the operation. Besides, the prepared BSA/anti-PTX-3/MAuNWs electrodes have excellent redox reversibility and stability. The biosensor has a wider detection range (0.001 ~ 1000 ng ml^{-1}) and a lower detection limit (0.16 pg ml^{-1}) than other detection methods. This paper reports the use of an electrochemical biosensor for direct detection of PTX-3 antigens. The biosensors proposed in this work can provide more reliable detection methods for clinical application because of their numerous advantages. MAuNWs/GCE biosensor platform can be used to construct more detection methods for clinically important biomarkers.

Supplementary Information The online version contains supplementary material available at https://doi.org/10.1007/s11581-021-03911-7.

References

1. Cao Y, Cong S, Cao X, Wu F, Liu Q, Amer MR, Zhou C (2017) Review of Electronics Based on Single-Walled Carbon Nanotubes. Top Curr Chem 375(5):75
2. Hemasa AL, Naumovski N, Maher WA, Ghanem A (2017) Application of carbon nanotubes in chiral and achiral separations of pharmaceuticals, biologics and chemicals. Nanomaterials (Basel) 7(7)
3. Duke KS, Bonner JC (2017) Mechanisms of carbon nanotube-induced pulmonary fibrosis: a physicochemical characteristic perspective. Wiley Interdiscip Rev Nanomed Nanobiotechnol 10(3): e1498

4. Snyder-Talkington BN, Qian Y, Castranova V, Guo NL (2012) New Perspectives for in Vitro Risk Assessment of Multiwalled Carbon Nanotubes: Application of Coculture and Bioinformatics. J Toxicol Environ Health B Crit Rev 15(7):468–492
5. Bajwa N, Li X, Ajayan PM, Vajtai R (2008) Mechanisms for Catalytic CVD Growth of Multiwalled Carbon Nanotubes. J Nanosci Nanotechnol 8(11):6054–6064
6. Sharma P, Mehra NK, Jain K, Jain NK (2016) Biomedical Applications of Carbon Nanotubes: A Critical Review. Curr Drug Deliv 13(6):796–817
7. Liang F, Chen B (2010) A Review on Biomedical Applications of Single-Walled Carbon Nanotubes. Curr Med Chem 17(1):10–24
8. Alshehri R, Ilyas AM, Hasan A, Arnaout A, Ahmed F, Memic A (2016) Carbon Nanotubes in Biomedical Applications: Factors, Mechanisms, and Remedies of Toxicity. J Med Chem 59(18): 8149–8167
9. Yin ZZ, Cheng SW, Xu LB, Liu HY, Huang K, Li L, Zhai YY, Zeng YB, Liu HQ, Shao Y, Zhang ZL, Lu YX (2017) Biosens Bioelectron 100:565–570
10. Wang Z, Wang K, Zhao L, Chai S, Zhang J, Zhang X, Zou Q (2017) A novel sensor made of Antimony Doped Tin Oxide-silica composite sol on a glassy carbon electrode modified by single-walled carbon nanotubes for detection of norepinephrine. Mater Sci Eng C Mater Biol Appl 80:180–186
11. Shoja Y, Rafati AA, Ghodsi J (2017) Enzymatic biosensor based on entrapment of d -amino acid oxidase on gold nanofilm/MWCNTs nanocomposite modified glassy carbon electrode by sol-gel network: Analytical applications for d -alanine in human serum. Enzym Microb Technol 100:20–27
12. Karimi-Maleh H, Amini F, Akbari A, Shojaei M (2017) Amplified electrochemical sensor employing CuO/SWCNTs and 1-butyl-3-methylimidazolium hexafluorophosphate for selective analysis of sulfisoxazole in the presence of folic acid. J Colloid Interface Sci 495:61–67
13. Ning L, Zhu B, Gao T (2017) Gold nanoparticles: promising agent to improve the diagnosis and therapy of cancer. Curr Drug Metab 18(11):1055–1067
14. Zhai TT, Ye D, Zhang QW, Wu ZQ, Xia XH (2017) Highly Efficient Capture and Electrochemical Release of Circulating Tumor Cells by Using Aptamers Modified Gold Nanowire Arrays. ACS Appl Mater Interfaces 9(40):34706–34714
15. Li N, Zhao P, Astruc D (2014) Anisotropic Gold Nanoparticles: Synthesis, Properties, Applications, and Toxicity. Angew Chem Int Ed Eng 53(7):1756–1789
16. Fan Z, Huang X, Chen Y, Huang W, Zhang H (2017) Facile synthesis of gold nanomaterials with unusual crystal structures. Nat Protoc 12(11):2367–2378
17. Balasubramanian S, Sheelam A, Ramanujam K, Dhamodharan R (2017) Green, Seed-Mediated Synthesis of Au Nanowires and Their Efficient Electrocatalytic Activity in Oxygen Reduction Reaction. ACS Appl Mater Interfaces 9(34):28876–28886
18. Niu Z, Cui F, Yu Y, Becknell N, Sun Y, Khanarian G, Kim D, Dou L, Dehestani A, Schierle-Arndt K, Yang P (2017) Ultrathin Epitaxial Cu@Au Core–Shell Nanowires for Stable Transparent Conductors. J Am Chem Soc 139(21):7348–7354
19. Schutt F, Postica V, Adelung R, Lupan O (2017) Single and Networked ZnO–CNT Hybrid Tetrapods for Selective Room-Temperature High-Performance Ammonia Sensors. ACS Appl Mater Interfaces 9(27):23107–23118
20. Wang S, Guan BY, Yu L, Lou XWD (2017) Rational design of threelayered TiO2 @Carbon@MoS2 hierarchical nanotubes for enhanced lithium storage. Adv Mater 29(37)
21. Saljooqi A, Shamspur T, Mostafavi A (2017) Ag-4-ATP-MWCNT electrode modified with dsDNA as label-free electrochemical sensor for the detection of daunorubicin anticancer drug. Bioelectrochemistry (Amsterdam, Netherlands) 118:161–167
22. Lech M, Rommele C, Anders HJ (2013) Pentraxins in nephrology: C-reactive protein, serum amyloid P and pentraxin-3. Nephrol Dial Transplant 28(4):803–811
23. Daigo K, Inforzato A, Barajon I, Garlanda C, Bottazzi B, Meri S, Mantovani A (2016) Pentraxins in the activation and regulation of innate immunity. Immunol Rev 274(1):202–217
24. Karnoub AE, VanHook AM (2017) Science SignalingPodcast for 21 February 2017: Pentraxin-3 in basal-like breast cancer. Sci Signal 10(467):eaam8855
25. Liu C, Yao Y, Wang W (2014) Pentraxin-3 as a prognostic marker in patients with small-cell lung cancer. Med Oncol 31(10):207
26. Huang XL, Zhang L, Duan Y, Wang YJ, Wang J (2016) Association of Pentraxin 3 with Autoimmune Diseases: A Systematic Review and Meta-Analysis. Arch Med Res 47(3):223–231
27. Zhang J, Wang TY, Niu XC (2016) Increased Plasma Levels of Pentraxin 3 Are Associated with Poor Prognosis of Colorectal Carcinoma Patients. Tohoku J Exp Med 240(1):39–46
28. Ma D, Zong Y, Zhu ST, Wang YJ, Li P, Zhang ST (2016) Inhibitory Role of Pentraxin-3 in Esophageal Squamous Cell Carcinoma. Chin Med J 129(18):2233–2240
29. dell'Oglio MP, Simone S, Ciccone M, Corciulo R, Gesualdo M, Zito A, Cortese F, Castellano G, Gigante M, Gesualdo L, Grandaliano G, Pertosa GB (2017) Neutrophil-dependent pentraxin-3 and reactive oxygen species production modulate endothelial dysfunction in haemodialysis patients. Nephrol Dial Transplant 32(9):1540–1549
30. Thukral R, Mangat S, Ganguly A, Agarkar SS, Bali H, Grover S (2017) Pentraxin-3 Levels in Gingival Crevicular Fluid during Canine Retraction with Nickel-Titanium Coil Spring and Active Tieback. J Contemp Dent Pract 18(8):710–713
31. Santilli F, Guagnano MT, Innocenti P, Aceto L, Vazzana N, Lattanzio S, Liani R, Tripaldi R, Creato V, Romano M, Davi G (2016) Pentraxin 3 and Platelet Activation in Obese Patients After Gastric Banding. Circ J 80(2):502–511
32. Zheng SD, Wu HJ, Yu SP, Ren JX, Duo WW, Ma ZC, Gao Y, Wang SQ, Liu YN (2015) Shenfu Injection suppresses inflammation by targeting haptoglobin and pentraxin 3 in rats with chronic ischemic heart failure. Chin J Integr Med 21(1):22–28
33. Campuzano S, Pedrero M, Pingarron JM (2017) Non-invasive breast cancer diagnosis through electrochemical biosensing at different molecular levels. Sensors (Basel, Switzerland) 17(9)
34. Yanez-Sedeno P, Campuzano S, Pingarron JM (2017) Multiplexed electrochemical immunosensors for clinical biomarkers. Sensors (Basel, Switzerland) 17(5)
35. Jin M, Zhang X, Zhen Q, He Y, Chen X, Lyu W, Han R, Ding M (2017) An electrochemical sensor for indole in plasma based on MWCNTs-chitosan modified screen-printed carbon electrode. Biosens Bioelectron 98:392–397
36. Yuan Y, Li S, Xue Y, Liang J, Cui L, Li Q, Zhou S, Huang Y, Li G, Zhao Y (2017) A Fe3O4@Au-basedpseudo-homogeneous electrochemical immunosensor for AFP measurement using AFP antibody-GNPs-HRP as detection probe. Anal Biochem 534:56–63
37. Liu Z, Ma Z (2013) Fabrication of an ultrasensitive electrochemical immunosensor for CEA based on conducting long-chain polythiols. Biosens Bioelectron 46:1–7
38. Sun S, Wang R, Huang Y, Xu J, Yao K, Liu W, Cao Y, Qian K (2019) Design of hierarchical beads for efficient label-free cell capture. Small 15(34):e1902441
39. Zhang R, Le B, Xu W, Guo K, Sun X, Su H, Huang L, Huang J, Shen T, Liao T, Liang Y, Zhang JXJ, Dai H, Qian K (2019) Magnetic "squashing" of circulating tumor cells on plasmonic substrates for ultrasensitive NIR fluorescence detection. Small Methods 3(2):1800474